

**UNITED STATES AIR FORCE
RESEARCH LABORATORY**

**FLASHBLINDNESS AND GLARE MODELING
OF OPTICAL RADIATION**

**William Kosnik
Peter Smith**

**Northrop Grumman Information Technology
4241 Woodcock Drive, Ste. B-100
San Antonio, TX 78228**

**HUMAN EFFECTIVENESS DIRECTORATE
DIRECTED ENERGY BIOEFFECTS DIVISION
OPTICAL RADIATION BRANCH
2650 LOUIS BAUER DRIVE
Brooks City-Base, TX 78235**

May 2003

Approved for public release; distribution unlimited.

20030701 107

NOTICES

This report is published in the interest of scientific and technical information exchange and does not constitute approval or disapproval of its ideas or findings.

This report is published as received and has not been edited by the publication staff of the Air Force Research Laboratory.


Using Government drawings, specifications, or other data included in this document for any purpose other than Government-related procurement does not in any way obligate the US Government. The fact that the Government formulated or supplied the drawings, specifications, or other data, does not license the holder or any other person or corporation, or convey any rights or permission to manufacture, use, or sell any patented invention that may relate to them.

The Office of Public Affairs has reviewed this paper, and it is releasable to the National Technical Information Service, where it will be available to the general public, including foreign nationals.

This report has been reviewed and is approved for publication.



LARRY J. SCHAD, Capt USAF
Contract Monitor



RICHARD L. MILLER, Ph.D.
Chief, Directed Energy Bioeffects Division

REPORT DOCUMENTATION PAGE

Form Approved
OMB No. 0704-0188

maintaining the data needed, and completing and reviewing this collection of information. Send comments regarding this burden estimate or any other aspect of this collection of information, including suggestions for reducing this burden to Department of Defense, Washington Headquarters Services, Directorate for Information Operations and Reports (0704-0188), 1215 Jefferson Davis Highway, Suite 1204, Arlington, VA 22202-4302. Respondents should be aware that notwithstanding any other provision of law, no person shall be subject to any penalty for failing to comply with a collection of information if it does not display a currently valid OMB control number. **PLEASE DO NOT RETURN YOUR FORM TO THE ABOVE ADDRESS.**

1. REPORT DATE (DD-MM-YYYY) May 2003		2. REPORT TYPE Final		3. DATES COVERED (From - To) 1997-2003	
4. TITLE AND SUBTITLE Flashblindness and Glare Modeling of Optical Radiation				5a. CONTRACT NUMBER F41924-97-D-9000	
				5b. GRANT NUMBER	
				5c. PROGRAM ELEMENT NUMBER 62202F	
6. AUTHOR(S) William Kosnik and Peter Smith				5d. PROJECT NUMBER 7757	
				5e. TASK NUMBER B2	
				5f. WORK UNIT NUMBER 04	
7. PERFORMING ORGANIZATION NAME(S) AND ADDRESS(ES) Northrop Grumman Information Technology 4241 Woodcock Drive, Suite B100 San Antonio, TX 78228				8. PERFORMING ORGANIZATION REPORT	
9. SPONSORING / MONITORING AGENCY NAME(S) AND ADDRESS(ES) Human Effectiveness Directorate Directed Energy Bioeffects Division Optical Radiation Branch 8111 18 th Street Brooks City-Base, TX 78235-5215				10. SPONSOR/MONITOR'S ACRONYM(S) AFRL/HEDO	
				11. SPONSOR/MONITOR'S REPORT NUMBER(S) AFRL-HE-BR-TR-2003-0069	
12. DISTRIBUTION / AVAILABILITY STATEMENT Approved for public release; distribution is unlimited					
13. SUPPLEMENTARY NOTES					
14. ABSTRACT This paper reports on a mathematical model of the visual effects of optical radiation. This model is a part of the AFRL/HEDO Laser Threat Modeling Component (LTMC) laser hazard bioeffects application. It estimates the temporary reduction in visual sensitivity caused by non-damaging optical radiation sources, especially lasers. Even at low power, lasers produce intense radiation that can significantly disrupt visual function. The model analyzes the factors involved in a laser exposure incident including the optical exposure parameters, the role of atmospheric attenuation, the ambient environment, the optics of the eye, and the visual task. The scientific bases of the algorithms are presented and the appropriate research literature is reviewed. The strengths and weaknesses of the approaches are compared and evaluated in terms of their applicability to AF optical radiation concerns.					
15. SUBJECT TERMS Flashblindness, Glare, Laser, Optical Radiation, Dark adaptation, Light adaptation, Model					
16. SECURITY CLASSIFICATION OF:			17. LIMITATION OF ABSTRACT	18. NUMBER OF PAGES	19a. NAME OF RESPONSIBLE PERSON
a. REPORT	b. ABSTRACT	c. THIS PAGE			Robert Thomas
Unclass	Unclass	Unclass	UL	48	19b. TELEPHONE NUMBER (include area code) (210) 536-6558

Table of Contents

Introduction.....	1
Laser Threat Modeling Component Application	2
LTMC Glare Model	2
Photometric quantities	2
Optical source considerations	3
Retinal distribution of a point source.....	4
The equivalent background luminance	5
Computing glare effects on target visibility.....	7
Target considerations	8
Wavelength effects	10
LTMC Flashblindness Model	11
Pupil size.....	11
Time-intensity relationships of flash brightness	12
Time-intensity relationships in flashblindness recovery	14
Flashblindness Recovery Functions.....	15
Comparison of the flashblindness functions.....	17
A Test of the Flashblindness Recovery Functions.....	22
Summary	24
Recommendations.....	25
References.....	26
Appendix A.....	30
Appendix B	33
Appendix C	36
Appendix D.....	39

List of Figures

Figure 1. The CIE photopic spectral luminosity curve for the standard observer (1926).....	3
Figure 2. A schematic diagram of the human eye showing how light from a distant source forms an image on the retina.....	4
Figure 3. The point spread function describing intraocular light scatter in the human eye.....	6
Figure 4. The VIDEM model predicts the detectability of aircraft against a daytime sky background (Akerman & Kinzly, 1979).....	9
Figure 5. HUD and HDD symbol contrast thresholds as a function of adapting background luminance level.....	10
Figure 6. Pupil diameter determined by ambient adapting luminance, adapted from de Groot and Gebhard (1952).	12
Figure 7. An idealized threshold-duration function (Bloch's law).....	13
Figure 8. The forms of the three flashblindness recovery functions for an input flash energy of 7.6 log td·s.....	16
Figure 9. Derivation of the offset parameter, c , in the Menendez-Smith function.....	17
Figure 10. Results of the parameter estimation exercise using the Smith (1996) data.....	19
Figure 11. Parameter estimates obtained from fitting the Smith function to Smith's (1996) flashblindness data.....	20
Figure 12. Parameter estimates obtained from fitting the Hahn-Geisler function to Smith's (1996) flashblindness data.....	21
Figure 13. The fit of the three functions to the Smith (1996) flashblindness recovery data for three flash energies.....	23
Figure 14. The three decay functions are plotted against the Menendez and Garcia (1985) flashblindness recovery data.....	24

List of Tables

Table 1. Supplemental target database for use in specifying HUD-like symbology.....	10
Table 2. Empirically derived free parameter estimates of the Smith and Hahn-Geisler functions.	18
Table 3. Predicted estimates of the free parameters in the Smith and Hahn-Geisler functions.	21

Acknowledgments

The authors thank their colleagues, Leon McLin and Fred Previc, for their help and support in developing the models and producing this manuscript. The authors acknowledge the support of the Optical Radiation Branch of the US Air Force Research Laboratory via contract, F41624-97-D-9000, awarded to TASC.

Introduction

The use of lasers in Air Force (AF) operations is increasing rapidly (Scott, 1999), and the deployment of low-power lasers as anti-personnel weapons is a growing threat to AF aircrews (Mellerio, Marshall, Tengroth, Anderberg, & Wolbarsht, 1991). Consequently, the possibility of a loss in vision resulting from an accidental or hostile laser exposure continues to increase year after year. The Air Force Research Laboratory Optical Radiation Branch (AFRL/HEDO) has been studying this problem for over two decades. This effort has led to the creation of mathematical models that describe how basic visual processes are affected by exposure to optical sources, such as lasers. Such models are important because they help analysts understand how a functional visual deficit impacts aircrew performance and ultimately mission success.

Exposure to a visible laser beam can cause temporary visual impairment, such as glare and flashblindness, without producing physical eye damage. AFRL/HEDO has developed models of these effects. The Glare Model is principally based on the work of Vos and others at the TNO Human Factors Research Institute (Vos, 1984; Vos & van den Berg, 1997). The Flashblindness Model was originally developed by Menendez and Smith (1990) at AFRL/HEDO. Though related, the models are distinguished by the timing of the optical radiation source - the Glare Model estimates the visual impairment during the laser exposure, while the Flashblindness Model predicts residual effects after the exposure.

This report reviews the state of glare and flashblindness modeling at AFRL/HEDO. The scientific basis of the algorithms is presented and the appropriate research literature is reviewed. The strengths and weaknesses of the approaches are compared and evaluated in terms of their applicability to AF optical radiation concerns. In addition, issues that relate to the assumptions, validity, and scope of the models are addressed. These issues include short pulse exposures, multiple pulse exposures, and the impact of exposure intensity and duration on light adaptation.

The Glare Model is presented first. The major components of the model are presented, including optical radiation source parameters, transmission of light through the eye, the principle of the equivalent background, the concept of veiling glare, and target considerations. The report continues with a discussion of the Flashblindness Model. The Flashblindness Model includes all of the components in the Glare Model with the addition of a flashblindness recovery function that describes the process of dark adaptation. Three candidate algorithms for the flashblindness recovery function are discussed and compared. The current model (Menendez & Smith, 1990) is compared to two alternative models - an updated one by Smith (1996) and one adapted from Hahn and Geisler (1995). The model that best represented the experimental flashblindness recovery data was incorporated in LTMC. Finally, recommendations to further develop and improve the Glare and Flashblindness Models are made.

Laser Threat Modeling Component Application

The Flashblindness and Glare Models are parts of the Laser Threat Modeling Component (LTMC) application. LTMC is the flagship laser hazard bioeffects model of AFRL/HEDO. LTMC is a Microsoft Windows NT™-based integrated modeling and simulation environment that helps analysts evaluate the vulnerability of aircrew to optical radiation threats in operational and training environments. LTMC is composed of a set of modular software components that provides hazard evaluations, classification and range calculations for optical radiation bioeffects including eye damage, flashblindness, and glare. The Flashblindness and Glare Models provide estimates of reductions in visual sensitivity as a function of distance from the optical source. This information allows mission planners to assess aircrew vulnerability during a mission profile.

LTMC Glare Model

The Glare Model determines how the visibility of a target is degraded by glare. For this analysis the model uses quantitative measures of the source exposure, the target and background scene brightness, and the visibility threshold of the target of interest. The model first converts the source exposure from radiometric units into photometric units. An intraocular scatter function describes how the light source is distributed on the retina after passing through the ocular media. The scatter function transforms the source into a glare field of a given luminance distribution. The glare field produces a relative scotoma, that is, an area of reduced visual sensitivity in the field of view. The scotoma is formed by superimposing the glare field onto the target and background scene, which reduces scene contrast. The model compares the reduced target contrast to the target visibility threshold and determines if the target has been obscured. A detailed description of the Glare Model follows beginning with the radiation source.

Photometric quantities

Although laser sources are usually described in terms of radiometric quantities, these give no indication of the effectiveness of the source as a stimulus for vision. The photometric system was developed to describe optical radiation in terms of its ability to elicit a response from the visual system. The basic photometric unit of luminous power, or luminous flux, is the lumen (lm). The lumen is the photometric equivalent of the watt (W). Under photopic conditions, one watt of radiant flux at 555 nm is, by definition, equivalent to 685 lm of luminous flux. This wavelength is at the peak of the spectral sensitivity of the eye under photopic viewing conditions. The relative sensitivity of the eye is defined by the *Commission Internationale de l'Eclairage (CIE)* (1926) relative photopic¹ spectral luminosity function, V_λ , for a standard observer (Figure 1). This function is given a value of unity at 555 nm, its maximum.

For a laser with a radiant flux of P (in W) at 555 nm, the luminous flux is $685 \times P$ lm. To generalize to any laser wavelength, λ , the luminous flux, ϕ , is calculated as:

¹ The photopic function is used because photopic, or cone vision, is used for essentially all aircrew visual functions.

$$\phi = 685 \times P \times V_{\lambda}, \quad (1)$$

where P is the radiant flux, and V_{λ} is the value of the relative spectral luminosity function at this wavelength.

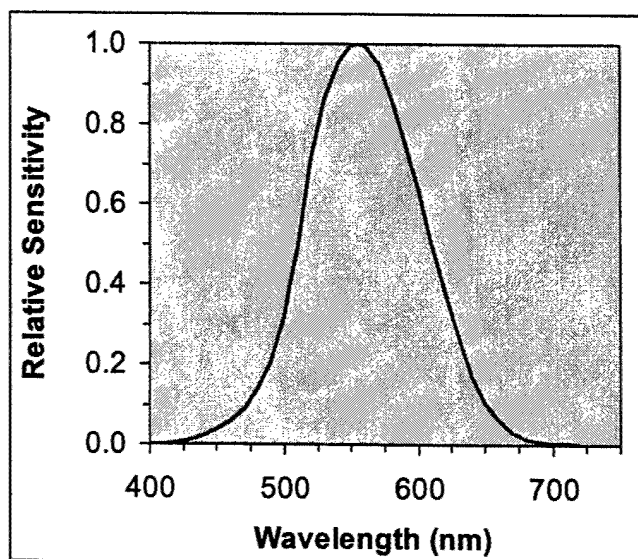


Figure 1. The CIE photopic spectral luminosity curve for the standard observer (1926). The curve shows peak sensitivity at 555 nm and declines toward zero at 400 and 750 nm.

Optical source considerations

The Glare Model analyzes glare effects for continuous wave (CW), single wavelength, point source exposures, based on the source irradiance measured at the cornea. The photometric equivalent of irradiance is illuminance, E_v (in $\text{lm} \cdot \text{m}^{-2} \equiv \text{lux}$), which is related to irradiance, E_e (in $\text{W} \cdot \text{cm}^{-2}$), by:

$$E_v = 685 \times E_e \times V_{\lambda} \times 10^4. \quad (2)$$

In addition, since the human visual system perceives a flickering light source with a frequency above 60 Hz as continuous (Brindley, 1960), the effects of pulsed laser systems with pulse repetition frequencies greater than 60 Hz can also be analyzed. For these sources, the irradiance is given by the time-averaged irradiance.

A schematic view of the eye is shown in Figure 2. Light rays from a distant optical source are focused on the retina and are concentrated approximately 50,000 times (Sloney & Wolbarsht, 1976). This is what makes a visible laser so potentially damaging to ocular tissue compared to skin tissue. Most lasers, when viewed from a distance, are considered point sources, because they appear to have little or no spatial extent. The American National Standards Institute (ANSI) provides guidelines for determining whether a laser may be considered a point or an extended source (American National Standards Institute, 2000). The standard defines a laser that subtends an angle less than

some minimum angle at the eye as a point source. The criterion minimum angle depends on exposure duration, but when the source produces an image on the retina of 20-30 μm in diameter, and is nearly diffraction-limited, then it is generally considered a point source.

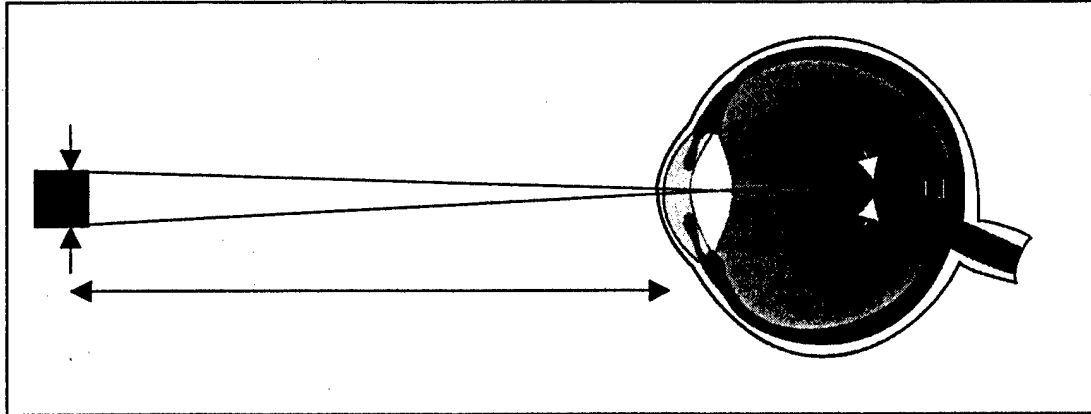


Figure 2. A schematic diagram of the human eye showing how light from a distant source forms an image on the retina. If the source subtends an angle less than the critical angle, α , then it is considered a point source.

Retinal distribution of a point source

Although the light from a point source should be imaged on the retina as a point, in reality, the focused rays do not all converge on one spot. Optical imperfections such as spherical and chromatic aberrations, diffraction effects, and refractive errors, cause the image of a point of light to be blurred on the retina (Campbell & Green, 1966; Campbell & Gubisch, 1966; Vos, 1984; Westheimer, 1986). Retinal image quality is further degraded by intraocular stray light from internal ocular reflections.

Estimates of the extent of laser glare, therefore, must begin with a calculation of how the laser light is distributed on the retina. The precise shape of the retinal distribution has been a topic of great interest in applied vision work related to veiling glare and there has been a concerted effort to quantify it. A number of studies have been compiled and analyzed by Vos and Berg (1997) who have produced an analytical expression for the point spread function (PSF) that closely fits most available data, distinguishes the different components of entoptic scatter, and explicitly depends on age and complexion. The expression breaks the sources of intraocular scatter into three components: an anterior component from the cornea and lens; a wall component from the iris and sclera; and an epithelium component for scatter from the retinal pigment epithelium (RPE). The *PSF* describes a radially symmetric distribution of light on the retina as a function of angular distance, θ (in degrees), from the center of the source:

$$PSF(\theta) = Anterior(\theta) + Wall(\theta) + Epithelium(\theta) \quad (3)$$

The expression for scatter by the anterior segment contains an age factor (Ijspeert, de Waard, van den Berg, & de Jong, 1990; Ijspeert, van den Berg, & Spekreijse, 1993; van Meeteren, 1974) and is given by:

$$Anterior(\theta) = 1.03 \times \left(1 - 0.1 \left(\frac{A}{70}\right)^4\right) \left(\left(\frac{8.83 \times 10^6}{\left(1 + \left(\frac{\theta}{0.0046}\right)^2\right)^{1.5}} \right) + \left(\frac{1.43 \times 10^5}{\left(1 + \left(\frac{\theta}{0.045}\right)^2\right)^{1.5}} \right) \right) + 0.46 \left(1 + 1.85 \left(\frac{A}{70}\right)^4\right) \left(\frac{10^3}{1 + \left(\frac{\theta}{0.1}\right)^2} + 7 \times 10^{-8} \theta^2 \right), \quad (4)$$

where A is the person's age in years and θ is the glare angle in degrees.

The amount of light passing through the iris and sclera is given by:

$$Wall(\theta) = 3.5 \times 10^{-5} \left(\frac{105 - \theta}{\cos(0.92(\theta - 5))} \right). \quad (5)$$

The magnitude of the epithelial is component depends on the degree of pigmentation, with a heavily pigmented RPE scattering less light than a lightly pigmented one, and is given by:

$$Epithelium(\theta) = 0.175P \left(\left(\frac{16}{(\theta + 0.1)^3} \right) + \left(\frac{1}{(\theta + 0.1)} \right) \right) \quad (6)$$

where P is the pigmentation of the eye, which varies from 0 in heavily pigmented non-Caucasians, to 1.2 for very light-eyed Caucasians (van den Berg, 1995). The variation in the PSF due to age (in the typical range for aircrew) and pigmentation is small, so a general function is used in the Glare Model (Figure 3), which is based on a 30 year old, brown-eyed Caucasian ($P=0.75$).

Another algorithm has been developed that estimates the retinal light distribution from an extended light source (Toet, Ijspeert, Vos, & Walraven, 1995). This algorithm convolves the PSF with an extended light source to predict a two-dimensional retinal light distribution. When added to LTMC, this algorithm will be able to predict the effects of extended light sources, such as exposures passing through optical media (e.g. aircraft canopies).

It is known that intraocular scatter increases when light enters the eye obliquely, that is, not parallel to the visual axis. Oblique scatter increases appreciably when the angle of incidence exceeds about 20° (Jennings & Charman, 1981). However, because the Glare Model assumes the point source is always parallel to the visual axis, no corrections are necessary for obliquely incident light.

Since the Glare Model is a static model, it assumes that the glare source and target are fixed in space and time. It does not account for eye movements, which means that glare effects are fixed with respect to retinal location.

The equivalent background luminance

The effort to measure the effect of a glare source on the retina has a long history (Vos, 1963, 1984). In an early paper Cobb (1911) introduced the concept of the equivalent background luminance (EBL) to extrapolate the effect of a glare source to a wide variety of visual tasks. He showed that vision in the presence of a glare source was

impaired as if a veil of light were cast over the targets in the field of view. The visual effect of the source could be described by equating the glare intensity at an angular distance on the retina to a uniform distribution of light in visual space. The two were said to be equal when both sources had the same masking effect on a target of a specific

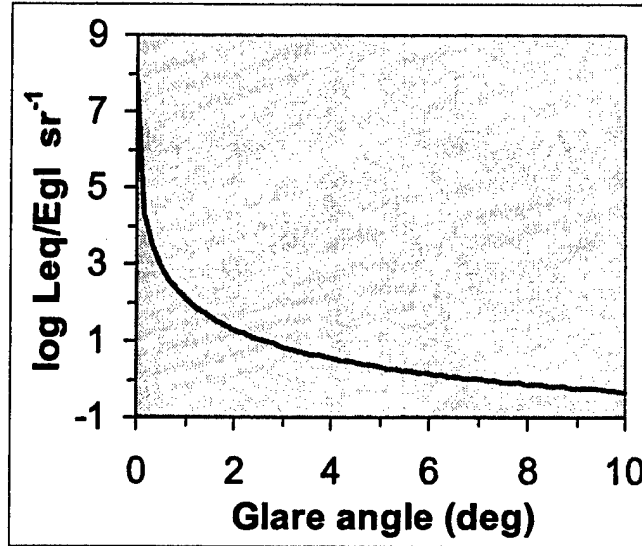


Figure 3. The point spread function describing intraocular light scatter in the human eye. The PSF is radially symmetric about the visual axis (0°) and is shown here for a 30-year old brown-eyed Caucasian.

luminance. Thus, the intensity of a glare source at any point along its profile could be expressed as a quantifiable light veil external to the eye. This comparison was performed psychophysically, where an observer looked at a point a certain angle from the center of the glare source and adjusted the brightness of an extended light source that had a comparable masking effect on a given target. This process was repeated over a range of angles to provide an EBL distribution of the glare source². The results were usually expressed as a *PSF* by plotting the equivalent luminance of the glare, L_{eq} , relative to the incident illumination from the glare source, E_{gl} ³.

$$PSF(\theta) = \frac{L_{eq}}{E_{gl}} \quad (7)$$

where L_{eq} is given in $\text{cd}\cdot\text{m}^{-2}$ and the illuminance of E_{gl} is in $\text{lm}\cdot\text{m}^{-2}$.

² The fact that the ratio of the glare source intensity to the equivalent background luminance was constant over a wide range of intensities supports the argument that the source of the glare was scatter from optical surfaces, and not neural in nature (Vos, 1984).

³ In photometric units, this is expressed in units of sr^{-1} (derived from $\text{cd}\cdot\text{m}^{-2}$ per lux, which is equivalent to $\text{lm}\cdot\text{sr}^{-1}\cdot\text{m}^{-2}$ per $\text{lm}\cdot\text{m}^{-2}$).

By simple rearrangement of Equation (7), the retinal distribution of a glare source can be expressed as an EBL profile by multiplying the glare illumination at the cornea by the *PSF*:

$$L_{eq} = E_{gl} \times \text{PSF}(\theta). \quad (8)$$

The advantage of stating the glare source in terms of an EBL is that the EBL can be expressed in the same brightness units (e.g., $\text{cd}\cdot\text{m}^{-2}$) as targets and backgrounds. In this way glare can simply be added to the target and background to determine its effect on target visibility.

The Glare Model limits the glare intensity as well. An upper limit is based on the premise that if all of the photopigment is bleached by a given exposure, then any additional light has no effect on the light adapted state of the eye. There is general agreement that a $7.6 \log \text{td}^4$ exposure bleaches 100% of the photopigment (Rushton & Henry, 1968). Any additional photons are not absorbed and, therefore, do not result in a change in sensitivity or in light adaptation. Thus, $7.6 \log \text{td}$ was set as the limit for modeling glare intensity⁵. The next section discusses the way target visibility is reduced by glare.

Computing glare effects on target visibility

Once the light distribution of the glare source on the retina is computed and expressed in terms of an EBL, then the effect on target contrast can be estimated.

The contrast, C , of a target in the visual scene is computed as:

$$C = \frac{|T - B|}{B}, \quad (9)$$

where T is the target luminance and B is the background luminance, both of which are expressed in $\text{cd}\cdot\text{m}^{-2}$. The absolute value of the difference between the target and background luminance is taken because the difference in the visibility of positive contrast and negative contrast targets is negligible.

The superimposition of the veiling glare source is expressed mathematically by adding the *EBL* to the target luminance and background luminance quantities. The apparent target contrast, C' , in the presence of the glare source is given as:

$$C' = \frac{|(T + \text{EBL}) - (B + \text{EBL})|}{B + \text{EBL}} = \frac{|T - B|}{B + \text{EBL}}. \quad (10)$$

The veiling luminance from the glare source does not, therefore, affect the difference between the target luminance and the background luminance, but provides an elevated background against which this luminance difference must be viewed and, hence, reduces target contrast. Since the glare decreases with angular distance from the center of

⁴ A troland is defined as the retinal stimulation provided by a source of $1 \text{ cd}\cdot\text{m}^{-2}$ viewed through a pupil of area of 1 mm^2 .

⁵ The Glare Model assumes a one-second exposure.

the image of the source, that is, EBL is a function of θ (Equation 8), the apparent target contrast must be computed at each retinal location across the glare profile. The Glare Model assumes that the target and the veiling glare are radially symmetric so the apparent target contrast is only computed along one meridian.

To determine whether the glare source obscured the target, the apparent target contrast is compared to the target contrast threshold. The procedure must be carried out for each point along the retinal meridian. If the apparent target contrast is below the contrast threshold, then the target is not visible at that point. The target is considered obscured when the target is below threshold across its entire extent.

Target considerations

The Glare Model assumes that the observer is looking directly at the target and that the optical source is close enough to the target so that the images are effectively coincident. Thus, both the target and the peak of the glare source are centered on the fovea. This arrangement yields the maximum likelihood of obscuring the target and represents a worst-case scenario for target detection.

Targets are expected to be small in angular extent, because they are usually viewed from long range. Therefore, target detection algorithms that pertain to small, spot targets are appropriate for use in the model. The default target detection algorithm is from the visual detection model, VIDEM, a model created for predicting aircraft detectability (Akerman & Kinzly, 1979). The algorithm estimates the contrast necessary for the target to be just visible (50% probability detection criterion) against an unstructured, uniform background. The algorithm is based on a set of laboratory contrast threshold tests (Lamar, Hecht, Schlaer, & Hendley, 1947, 1948; Sloan, 1961), which were then validated by aircraft detection field tests. Using these data Akerman and Kinzly (1979) found that the contrast threshold, C_t , was best described by the following function:

$$C_t = 0.0352 \times \theta^{0.24} + \frac{0.584 \times \theta^{1.6}}{\alpha^2} \quad (11)$$

where θ is the distance of the target from the fovea center (in degrees) and α is the target size (in minutes-of-arc).

Figure 4 shows a family of VIDEM contrast thresholds for various target sizes and angular distances from the fovea. The VIDEM algorithm was developed to predict the contrast threshold for detection of aircraft against daytime sky background using aircraft size and retinal location as variables and assumes that the target is small and circular in shape. If the target is not circular, then the target must be expressed in terms of an equivalent circular area.

One limitation of VIDEM is that the peripheral threshold data are all based on a single level of background adaptation ($10 \text{ cd}\cdot\text{m}^{-2}$). This level would be appropriate for detecting aircraft just after dawn and just before dusk. Indeed, increment-detection measures indicate that Weber's law of constant thresholds begins around $10 \text{ cd}\cdot\text{m}^{-2}$ for small spot targets (Blick, Beer, Kosnik, Troxel, Toet, Walraven, & Mitchell, 2001). This implies that contrast thresholds are the same at higher adaptation levels and no adjustment for higher background luminance levels is necessary. However, contrast thresholds are

higher at luminance levels below $10 \text{ cd}\cdot\text{m}^{-2}$ (Smith, 1996), and this argues for an expansion of the VIDEM database if detection thresholds for lower adaptation levels need to be estimated.

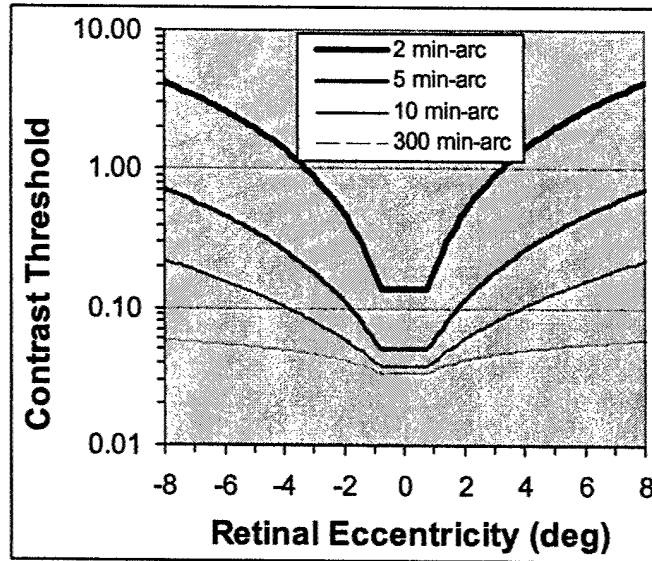


Figure 4. The VIDEM model predicts the detectability of aircraft against a daytime sky background (Akerman & Kinzly, 1979). Contrast thresholds are based on target diameter in minutes of arc and retinal location in degrees. The model assumes radial symmetry of thresholds. Thresholds increase with eccentricity from the fovea starting at 0.8° , and as target size diminishes.

Other target threshold databases, which augment the VIDEM model, are available in the model when the visual task cannot be reduced to the detection of disk-like objects. Two inside-the-cockpit visual tasks were included: head-up display (HUD) and head-down display (HDD) symbols. The latter is representative of emissive CRT displays. HUD and HDD symbols differ slightly in their computations due to the way background light is treated. The contrast ratio is formed in the normal way (see Equation 9) for HDD symbols, but the background light is added back into the numerator for HUD symbols, so the contrast ratio is simply:

$$C = \frac{T}{B}. \quad (12)$$

For HUD symbols contrast threshold is calculated by:

$$C_T = 0.2667 \cdot e^{-(0.5555 \cdot \log(BL))} \quad (13)$$

where BL = Background Luminance in $\text{cd}\cdot\text{m}^{-2}$. For HDD symbols the contrast threshold is calculated as:

$$C_T = 10^{(m \cdot \log(BL) + b)} \quad (14)$$

where m and b take on values given in Table 1 according to the adapting background luminance level.

Table 1. Slope (m) and intercept (b) values over a range of adapting background luminances for determining HDD symbol contrast thresholds.

Background Luminance (cd m ⁻²)	≤4	≤40	≤1700	>1700
m	-.44	-.18	-.08	-.01
b	-.29	-.69	-.93	-1.16

Figure 5 shows how HUD and HDD contrast thresholds vary with adapting background luminance level. At low levels contrast threshold is high, but declines rapidly as luminance increases.

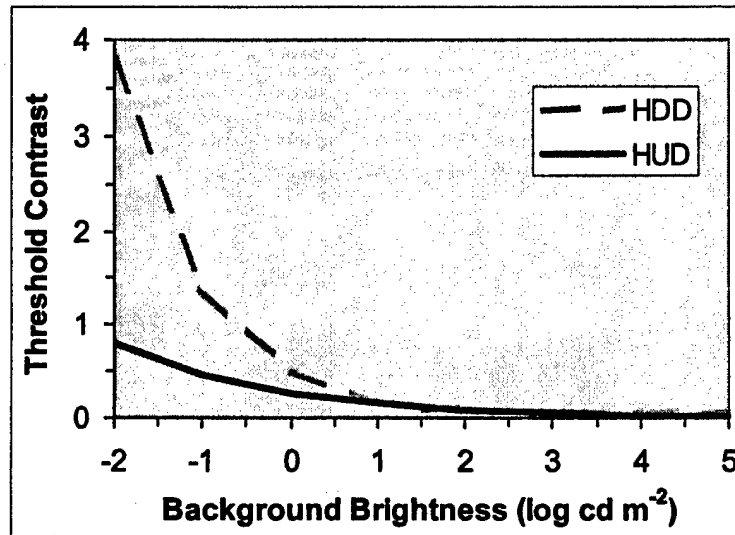


Figure 5. HUD and HDD symbol contrast thresholds as a function of adapting background luminance level. Contrast thresholds are high in the dark, but decrease rapidly as background luminance level increases. Dawn and dusk adapting levels are about 1 cd·m⁻², office light levels are about 100 cd·m⁻², and bright daylight levels are in the 10000 cd·m⁻² range.

Wavelength effects

Because lasers are monochromatic, possible wavelength effects on glare must be considered. Wavelengths may be scattered differently by the ocular media, such as in Rayleigh scattering. Although earlier investigations have presented contradictory results, more recent research indicates that entoptic scatter is not wavelength dependent, at least when extended sources are used (Wooten & Geri, 1987).

Another possible effect of wavelength on glare is through chromatic contrast. Targets of equal brightness may still be discriminable by a difference in color (Pokorny & Smith, 1986). Monochromatic laser light might interact with a target's color to produce differential effects on chromatic sensitivity. Indeed, several reports have shown

differential effects of wavelength on colored targets (Previc, 1987; Schmeisser, 1987; Varner et al., 1988). Responses to colored targets were reduced when the laser and the target were similar in color. However, these effects tended to be small compared to impact of the source brightness on colored target visibility. Consequently, the model does not incorporate wavelengths effects except for correcting the source irradiance for the chromatic sensitivity of the eye.

LTMC Flashblindness Model

Flashblindness is analyzed the same way as glare, except that the Flashblindness Model estimates recovery of visual sensitivity after the source has been turned off. As a result, the magnitude of the flashblindness effect depends on exposure duration. The Flashblindness Model analyzes effects for single-pulse, single wavelength, point sources. However, as with glare sources, multiple-pulse exposures greater than 60 Hz may also be analyzed as a single continuous pulse.

The model accepts optical radiation inputs in terms of a radiant exposure, H_e ($J \cdot cm^{-2}$) and exposure duration (s). The radiant exposure is measured at the cornea. The radiant exposure is converted to photometric units by the equation:

$$H_v = 685 \times H_e \times V_\lambda \times 10^4, \quad (12)$$

where H_v is the integrated illuminance in $lu \cdot m^{-2} \cdot s$.

The Flashblindness Model adds one more step to the Glare Model. This step represents a gradual return of visual sensitivity after the optical source as been turned off. Once the source has been extinguished, sensitivity begins to recover in a process known as dark adaptation. Just as the Glare Model, the Flashblindness Model uses the equivalent background principle to model the recovery in sensitivity (Crawford, 1947). Flash energy is again represented as a veil of light, but now one that fades with time. The initial step in the Flashblindness Model is the expression of the flash energy in terms of the integrated retinal illuminance. The PSF is applied to the flash energy to estimate the retinal distribution of the flash as an integrated luminance in $cd \cdot m^{-2} \cdot s$, that is, as an EBL times the exposure duration, t . Then the integrated luminance is expressed in terms of integrated retinal illuminance, L_v , in $td \cdot s$. This is done by multiplying L_{eq} by the area of the pupil, and the exposure duration:

$$L_v = PA \times L_{eq} \times t, \quad (13)$$

where L_{eq} is the EBL in $cd \cdot m^{-2}$, t is the exposure duration in s, and PA is the pupil area in mm^2 .

Pupil size

Pupil size is important because it determines the amount of light entering the eye, and, therefore, the retinal image brightness. It is also important because flashblindness studies quantify flash energy in terms of retinal illumination, so that input into the algorithm must be expressed in td . Pupil size is normally determined by the ambient level of illumination. The flashblindness source's duration of less than 150 ms would be too brief to elicit a sustained pupillary response. Therefore, the adapting background drives

pupil size in most situations. The model uses an algorithm developed by de Groot and Gebhard (1952) to estimate pupil size from adaptation level. The relation of pupil diameter to the brightness of an adapting light source is:

$$\text{Log } D = 0.8558 - 0.0004(\text{Log } B + 7.5972)^3 \quad (14)$$

where D is the pupil diameter in mm and B is the adapting field brightness in $\text{cd}\cdot\text{m}^{-2}$.

Figure 6 shows the association between pupil diameter and ambient luminance. The equation is the best fit to eight sets of data.

The model limits the possible range of pupil diameters between 2 and 7 mm. These limits were chosen because the adult pupil is not normally less than 2 mm and the ANSI standard for the estimation of laser ocular hazards uses a maximum of 7 mm to compute total intraocular energy (American National Standards Institute, 2000).

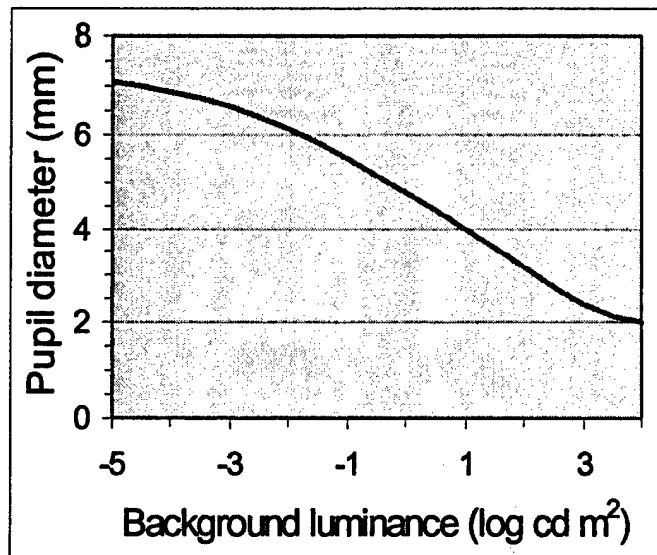


Figure 6. Pupil diameter determined by ambient adapting luminance, adapted from de Groot and Gebhard (1952). The model limits pupil diameter between 2 and 7 mm.

Time-intensity relationships of flash brightness

It is important for modeling purposes to accurately estimate the perceived brightness of the flash. The flash determines the initial adaptation level and, thus, the initial brightness of the EBL. As with glare, this can be done by comparing the flash illuminance to an EBL with the same masking effect. However, some care must be taken when doing this because the brightness of a flash depends on intensity *and* duration for brief lights. Common observation illustrates that the brightness of a steady light remains constant; it does not look brighter the longer one stares at it. However, if a light is turned on for a brief time, it looks dimmer the shorter the exposure duration. Therefore, time must be considered when estimating how bright a light flash looks.

A considerable body of evidence has shown that the visual system sums the intensity of light over time for short exposure durations (Hood & Finkelstein, 1986; Watson, 1986). This process of temporal integration is known as Bloch's Law. Bloch's Law states that the perceived brightness of a light is the product of its intensity and duration. However, this law is valid only up to a critical length of time. After that, no further summation takes place and brightness depends on intensity alone. This critical length of time is known as the critical duration. Bloch's Law may be stated mathematically as

$$I \times T = K \text{ for } T \leq T_c, \quad (15)$$

and

$$I = K \text{ for } T > T_c, \quad (16)$$

where I = intensity, T = time, K is a constant, and T_c is the critical duration. This law is an extension of the Bunsen-Roscoe law of photochemistry. A schematic diagram of Bloch's law is illustrated in Figure 7. In log-log coordinates, Equation (15) gives a straight line with a slope of -1.

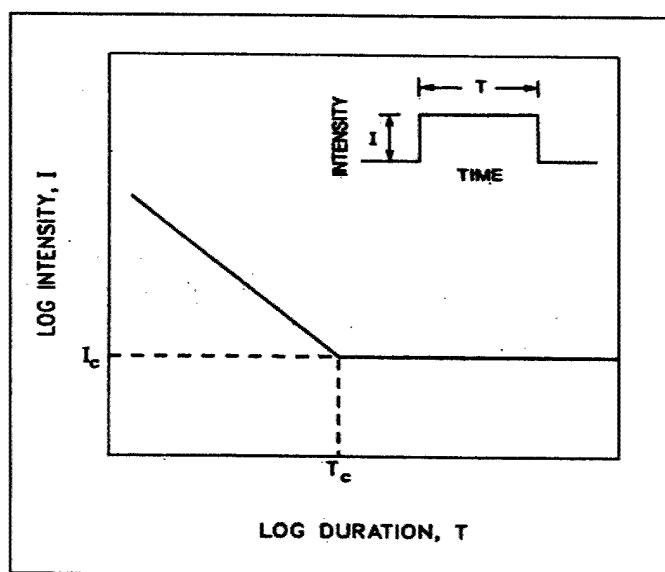


Figure 7. An idealized threshold-duration function (Bloch's law). The function describes thresholds for rectangular light pulses as a function of duration. The left limb of the function has a slope of -1 and the right limb has a slope of 0. The transition between the two limbs occurs at the critical duration T_c and the critical intensity I_c . The inset shows the wave form of a rectangular pulse with duration T and intensity I . From Watson (1986).

One consequence of this law is that lights of equal energy are equally detectable, that is, intensity and duration are reciprocal. Any combination of intensity and duration that yields a constant product appears equal in brightness. The intensity must be above the critical intensity and the duration must be below the critical duration. Equation (16) yields a horizontal line in Figure 7 and indicates that, after the critical duration, brightness

depends on intensity alone. When experimental data are considered, rarely do the two functions show such an abrupt shift from one slope to the other. Often a transition region is observed from complete reciprocity to no reciprocity. This region of partial summation is sometimes reported as having a -0.5 slope, and so follows an inverse-square law.

A number of studies have tried to pin down the exact length of the critical duration and have found that it is influenced by many factors including light adaptation level (Barlow, 1958; Crawford, 1937; Stewart, 1972), the size of the light (Barlow, 1958; Hood & Finkelstein, 1986; Karn, 1936), and wavelength (Sperling & Jolliffe, 1965). The shortest period of time for which reciprocity holds was investigated by Brindley (1952). He investigated equal energy suprathreshold lights between $0.4 \mu\text{s}$ and 8.9 ms and found that reciprocity was valid down to the shortest duration. Brindley was limited in the total energy he could deliver at the shortest durations because of the limited intensity of his light sources. As a result the $0.4 \mu\text{s}$ light was not very bright, only $0.3 \text{ td}\cdot\text{s}$. It would be beneficial to re-examine the reciprocity issue with brighter sources. Today's lasers with high peak power and short pulsewidths would be ideal to investigate the temporal integration properties of the visual system at heretofore-untested durations and intensities.

As a general rule one may conclude that reciprocity is valid up to a maximum time of about 150 ms in the cone system. Partial reciprocity occurs from $150\text{-}1000 \text{ ms}$ and brightness is largely independent of duration after 1 s (Kosnik, 1998; Watson, 1986). The following rule has been adopted for flashblindness modeling. The brightness of a flash is proportional to its energy for durations of 150 ms and less.

Time-intensity relationships in flashblindness recovery

Although reciprocity for brightness has been fairly well established, reciprocity in flashblindness recovery is not nearly so well understood. Consequently, a valid flashblindness model must establish some limits of reciprocity where equivalent energy exposures have the same effect on dark adaptation. Like brightness perception, the bulk of the evidence indicates reciprocity for short-duration exposures between 0.1 and 8.5 ms (Bowie & Collyer, 1973; Chisum, 1973; Miller, 1965). However, studies comparing millisecond and second durations generally did not find reciprocity (Bowie & Collyer, 1973; Crawford, 1946; Miller, King, & Schloessler, 1968). The evidence for durations between 10 ms and 1 s is mixed. Crawford (1946) found that durations between 9 and 900 ms showed reciprocity, more so for lower energy exposures than for higher ones. Bowie and Collyer (1973) found only partial reciprocity for durations between 13 and 100 ms and no reciprocity between 100 ms and 1 s . Thus, it appears that reciprocity is only found under a restricted set of conditions. For purposes of the model, therefore, equal-energy exposures having durations less than or equal to 150 ms are modeled with the same dark adaptation function. Although the literature is not in complete agreement on the higher end of this range, 150 ms is a reasonable limit because the eye blink reflex at 150 ms would prevent a continuous duration exposure from occurring anyway (Irving, 1960). Furthermore, eye movements would come into play after 150 ms , further distorting the shape of the retinal light distribution (Kosnik, 1988; Stamper, Lund, Molchaney, & Stuck, 2000). Therefore, the model handles most combinations of duration and intensity that would likely occur. Nevertheless, further research should be conducted to firmly establish the applicability of the reciprocity law in the range of 10 ms to 1 s .

The reciprocity rule is extended to include the integration of multiple pulses. Any train of pulses within 150 ms may be considered a single continuous pulse as far as flashblindness modeling is concerned. The individual pulses of a multiple pulse train are simply summed together. The flashblindness effect is considered the same no matter how the pulses are distributed. Furthermore, the model assumes that the visual system has reached a steady-state level of adaptation. Thus, it does not account for changing adaptation effects during the initial pulses of a multiple pulse train.

The Flashblindness Model also has an upper exposure limit. Based on the experimental evidence, which suggests that if all of the photopigment is bleached by a given exposure, then any additional energy has no effect on the light adapted state. The total energy of 7.6 log td·s was set as the upper limit as this exposure bleaches all of the photopigment (Rushton & Henry, 1968). This limit does not imply that higher energy flashes have no effect on other aspects of the model. For example, the retinal light distribution changes with higher energy flashes, and this aspect is modeled in the *PSF*.

Flashblindness Recovery Functions

AFRL/HEDO interest in visual recovery centers around exposure to lasers under operational conditions. Such exposures are de facto unintentional and it is safe to assume that the individual will make every effort to limit the exposure under most circumstances. Therefore, the model focuses on brief exposures. Visual recovery immediately following laser exposure is a primary concern to AFRL/HEDO. Air Force personnel most at risk for laser exposure are those engaged in critical tasks, such as flying an aircraft. The ability to maintain continuous flight control is of utmost importance. For this reason, visual recovery within the first two minutes is the focus of the modeling effort.

Three flashblindness recovery functions were considered for use in LTMC. The functions all have the same general form in that they express flashblindness recovery in terms of an equivalent background luminance (EBL), which decays as a function of time after the flash. Previous AFRL/HEDO flashblindness models have used a flashblindness recovery function developed by Menendez and Smith (1990). Smith later carried out extensive studies of flashblindness recovery in human subjects and developed a modified function (Smith, 1996). In addition, an exponential decay function is considered (Hahn & Geisler, 1995).

Just as in glare modeling, the equivalent background principle is a useful construct for describing the light adapted state of the eye; for flashblindness, the EBL includes a dark adaptation component as well (Crawford, 1947). Some have argued that the EBL represents the true state of adaptation at any time during dark adaptation (Crawford, 1947; Miller, 1965, 1966a, 1966b), but, this idea is still controversial (Hahn & Geisler, 1995; Hood & Finkelstein, 1986; Kosnik, 1998).⁶ One advantage of using the EBL for modeling

⁶The EBL has been compared to a flash afterimage, which has also been used to represent the light adapted state of the eye (Miller, 1966a, 1966b). The EBL can act like an afterimage under special circumstances. Both decrease in brightness with post-exposure time. However, the two are not the same (Barlow & Sparrock, 1964). The EBL, on the one hand, is a hypothetical construct. An afterimage, on the other hand, is a physiological phenomenon that has a perceptual counterpart. It can be positive or negative

flashblindness recovery is that it is independent of target and background conditions, so the flash effect can be generalized across all viewing conditions.

The Menendez-Smith (1990) function and the Smith (1996) function have the same general form. The functions relate the EBL magnitude to the initial flash energy as a function of time after the flash. Each function is a log-log equation of the form:

$$\text{Log } EBL = m \text{ Log } t + c, \quad (17)$$

where EBL is in $\text{cd}\cdot\text{m}^{-2}$ and t is time after the flash in s. The slope of the function, m , determines the rate at which the EBL fades and c is the offset. The difference between the two models is how they are parameterized.

The third function is based on the Hahn-Geisler (Hahn & Geisler, 1995) dark adaptation model. This model uses an exponential decay function to describe the dark adaptation process. It is based on the work of Rushton (1964; Rushton & Henry, 1968) and Hollins and Alpern (1973). The model was adapted to make it into the form of an EBL. Its general form is:

$$\text{Log}(EBL + 1) = \alpha e^{-t/t_c}, \quad (18)$$

where α is the initial light adaptation level at flash offset, t is time in s, and t_c is the time constant of decay. The EBL is continuous from the offset of the flash and decays to dark in this function. The forms of the three functions are shown in Figure 8 for a flash of 7.6 log td·s. Note that all three functions convert retinal flash energy into an external EBL.

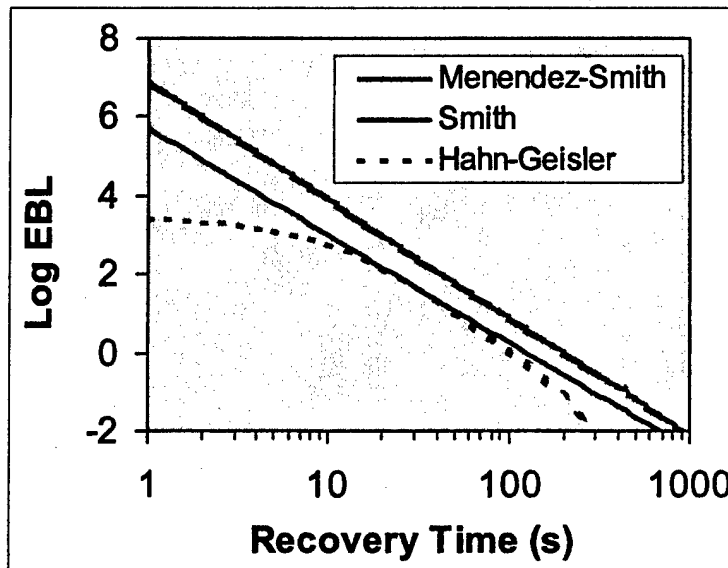


Figure 8. The forms of the three flashblindness recovery functions for an input flash energy of 7.6 log td·s.

(white or gray), or colored, and it can change in polarity and color with time. Its appearance depends on the background on which it is seen and it can be refreshed with eye blinks or eye movements.

Comparison of the flashblindness functions

The three functions were compared against a set of flashblindness data to determine which function best represented the flashblindness recovery process. First, though, the functions had to be parameterized. The Menendez-Smith function has two free parameters, m and c . The slope of the decay function, m , was assigned a value of -3 . This quantity is based on two studies by Miller (Miller, 1965, 1966b) who found that the log brightness of an afterimage faded at a rate of $-3 \log t$. Miller found that this rate was constant for flash energies between 6.68 and 7.48 log td·s. Menendez and Smith (1990) generalized this rate to all flash energies.

The offset, c , was determined by noting that $c = 3 \text{Log } t + 0.5$ when the EBL decayed to $3.2 \text{ cd}\cdot\text{m}^{-2}$. It was assumed that the target, a Sloan-Snellen letter, $0.22 \text{ cd}\cdot\text{m}^{-2}$ in brightness, was just resolvable when the EBL reached this level. In other words, the letter had a putative resolution threshold of 7%. Menendez and Smith (1990) used the results of Miller's (1965) flashblindness recovery data to determine at what time the EBL faded to the extent that the target reached threshold. Miller reported in her 1965 study five recovery times based on five different flash energies. By substituting the recovery times into Equation (17), Menendez and Smith (1990) derived five values for c . These values were plotted against flash energy to find a general expression for c . The results are shown in Figure 9. It can be seen that the c values form a straight line when plotted on a log-log chart. The best fitting line, fit by the least squares method, was:

$$c = 1.75F - 6.33, \quad (19)$$

where F is the flash energy in log td·s.

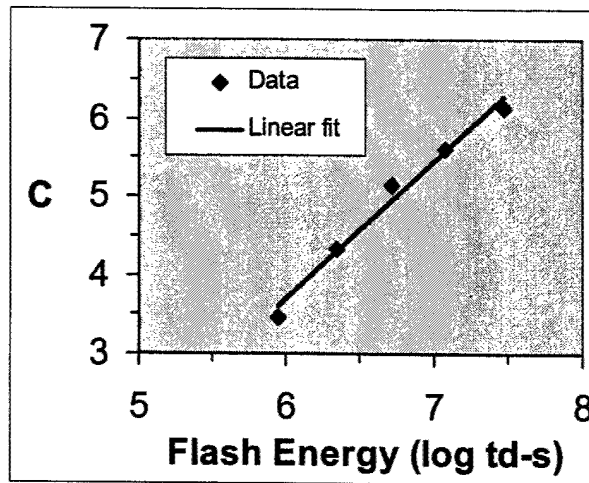


Figure 9. Derivation of the offset parameter, c , in the Menendez-Smith function. The coefficient, c , was derived from five recovery trials collected at five different flash energies. A general equation for c was obtained by fitting a linear function.

The coefficient of determination, R^2 , was 0.98, which indicated that the nearly all of the variation in the data was accounted for by the regression. Substituting for c , the decay function became:

$$\text{Log(EBL)} = -3\text{Log}(t) + 1.75F - 6.33, \quad (20)$$

The function was modified to limit flash energy to 7.6 log td·s and, thus, became:

$$\text{Log(EBL)} = -3\text{Log}(t) + 1.75 \times \min(7.6, F) - 6.33. \quad (21)$$

The Smith and Hahn-Geisler functions were parameterized using laser flashblindness recovery data from Smith (1996). This data set was chosen because it collected recovery times over a wide range of flash energies. Thus, the form of visual recovery could be assessed over a wide dynamic range. Recovery times were measured in two observers for identification of a 90% contrast Landolt C at seven background luminance levels ranging from 0.34 to 154 cd·m⁻². Ten laser flash energies were used ranging from 5.41 to 7.57 log td·s. The laser exposures were generated from the 514-nm line of a Coherent argon ion laser and were 100-ms in duration. Each exposure was presented as a circular, uniform Maxwellian-view spot subtending 1.15° at the eye. In addition, veiling luminance thresholds were measured at each of the background luminance levels and used to transform the recovery data into EBL versus time. These data, shown in Appendix A, were used to parameterize the functions.

The two free parameters in Equation (17), m and c , were fit simultaneously using the least squares method of linear regression. The solver function of Microsoft Excel™ performed the fitting procedure. Solver successfully converged on a solution in each case. The resulting estimated parameter values are shown in Table 2 for each flash energy.

The same procedure was used to parameterize the Hahn-Geisler function. Solver was used again to simultaneously fit the two free parameters, α and t_c , in Equation (18). Solver successfully converged on a solution and the resulting estimated values are shown in Table 2.

Table 2. Empirically derived free parameter estimates of the Smith and Hahn-Geisler functions.

Flash Energy Log (td·s)	Smith Function		Hahn-Geisler Function	
	m	c	α	t_c
5.41	-3.49	3.34	4.16	3.42
5.77	-3.02	4.06	3.58	8.88
6.12	-2.52	4.34	3.10	22.28
6.40	-2.80	4.87	3.41	22.13
6.67	-2.78	5.29	3.36	33.32
6.71	-2.72	5.23	3.37	33.54
6.94	-2.79	5.51	3.40	38.59
6.97	-2.70	5.40	3.36	39.97
7.27	-2.72	5.60	3.44	44.39
7.57	-2.56	5.26	3.52	39.73

Both functions fit the data well. All the residual errors from the least squares regression procedures were small. An example of the fits of the two functions for the 7.57 log td-s flash is shown in Figure 10. The results of the fitting procedure for the other flash energies are shown in Appendix B.

The fitting exercise showed that both functions simulated the flashblindness recovery process well. Nevertheless, it would be advantageous to find a general function that does not depend on data to estimate the free parameters. Thus, an attempt was made to express the free parameters in terms of flash energy. This was done by plotting the free

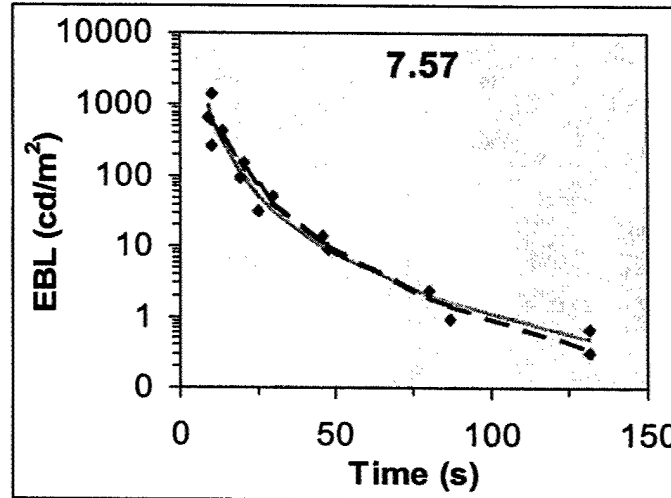


Figure 10. Results of the parameter estimation exercise using the Smith (1996) data. The plot shows the data from the 7.57 log td-s flash. The data are shown as the diamond symbols; the solid line is the Smith function and the broken line is the Hahn-Geisler function.

parameter values obtained in the data fitting exercise against flash energy and examining the results for trends. A least-squares regression procedure was used to derive equations for Smith's parameters, m and c . The parameter values obtained from the data fitting procedure are shown in Figure 11.

The squares indicate the slope parameter, m and the diamonds and circles show the offset parameter, c . The m term was fit by two straight lines. (See Smith, 1996, for the rationale for this approach.) The first four data points were fit by a straight line ($R^2 = 0.71$) of the form:

$$m = F - 8.92, \quad F < 6.11 \text{ log tds} \quad (22)$$

The rest of the data points were fit by the line ($R^2 = 0.03$):

$$m = -0.022F - 2.73, \quad F \geq 6.11 \text{ log tds.} \quad (23)$$

However, the slope of this line was not significantly different from zero so the equation reduced to the constant term, -2.73. The second parameter, c , was well fit ($R^2 = 0.99$) by

a second-order polynomial of the form:

$$c = 6.4F - 0.41F^2 - 19.43. \quad (24)$$

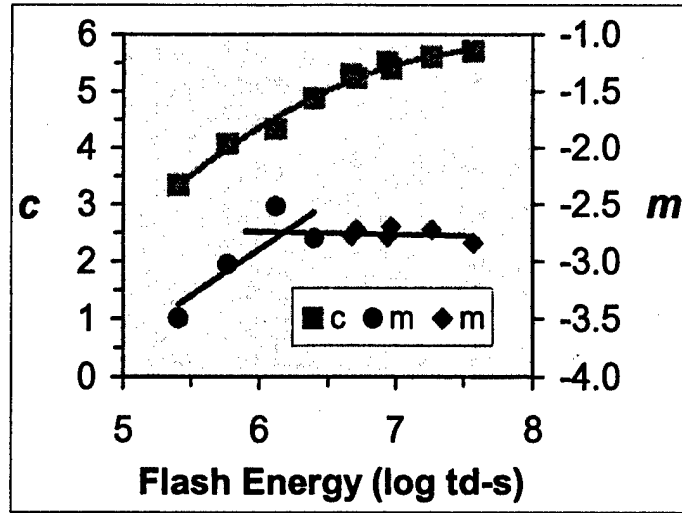


Figure 11. Parameter estimates obtained from fitting the Smith function to Smith's (1996) flashblindness data. The parameter estimates are plotted against flash energy. The offset parameter, c , is shown as the square symbols and uses the left ordinate. The diamonds and circles indicate the slope parameter, m , which uses the right ordinate. The three lines show the results of the curve-fitting procedures. The two solid lines show the linear trends for the m parameter and the dashed line shows the second order polynomial fit of the c parameter.

The plots of the two Hahn-Geisler parameters, α and t_c , are shown in Figure 12. The diamonds and circles show the α parameter and the triangles indicate the time constant parameter, t_c . As shown by Smith (1996), the α term was fit by two straight lines. The first three data points were fit by a straight line ($R^2 = 1.0$) of the form:

$$\alpha = -1.49F + 12.19, \quad F < 6.0 \log \text{td-s}. \quad (25)$$

The rest of the data points were fit with a line ($R^2 = 0.54$) of the form:

$$\alpha = 0.106F + 2.68, \quad F \geq 6.0 \log \text{td-s}. \quad (26)$$

The second parameter, t_c , was fit by a cumulative Gaussian function of the form:

$$t_c = \int_{F=0}^{7.6} k \left(\frac{(2\pi)^{-0.5}}{\sigma} \right) e^{-0.5 \left(\frac{F-\mu}{\sigma} \right)^2}, \quad (27)$$

where k is a constant and μ and σ are the mean and standard deviation of the distribution. This function was fit to the data by Solver. The function fit the data best ($R^2 = 0.97$) when $k = 43.23$, $\mu = 6.23$, and $\sigma = 0.60$. The cumulative Gaussian function seemed an appropriate model because it fit the limits of the flash energy. Flash energy cannot go below zero and it asymptotes after the photoreceptors become saturated, at about 7.6 log td-s (Rushton & Henry, 1968).

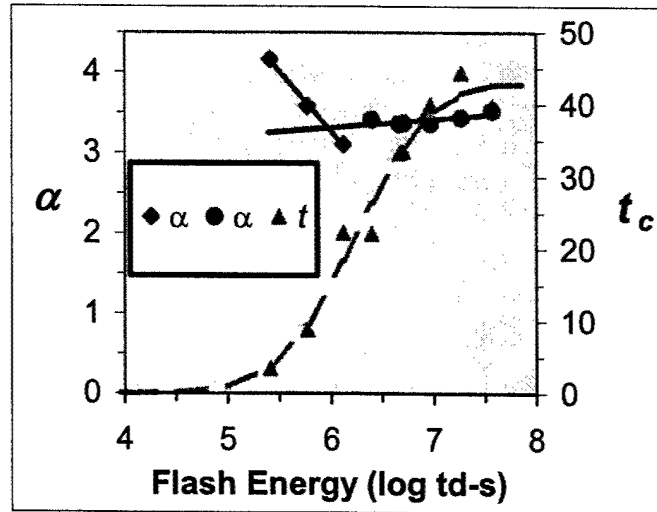


Figure 12. Parameter estimates obtained from fitting the Hahn-Geisler function to Smith's (1996) flashblindness data. The parameter estimates are plotted against flash energy. The α parameter, scaled by the left ordinate, is shown as the diamonds and circles. The triangles represent the time constant parameter, t_c , which is scaled by the right ordinate. The three lines show the results of the curve fitting procedures. The two solid lines show the linear trends for the α parameter and the dashed line shows the cumulative Gaussian fit of the time constant.

The flash energies were substituted back into the Equations (22-24) for the Smith function and Equations (25-27) for the Hahn-Geisler function to obtain model parameters at each flash energy. Table 3 shows the predicted model parameters.

Table 3. Predicted estimates of the free parameters in the Smith and Hahn-Geisler functions.

Flash Energy log td·s	Smith Function		Hahn-Geisler Function	
	Model <i>m</i>	Model <i>c</i>	Model α	Model t_c
5.41	-3.45	3.31	4.15	3.66
5.77	-3.08	3.97	3.61	9.52
6.12	-2.73	4.51	3.32	18.44
6.40	-2.73	4.88	3.35	26.44
6.67	-2.73	5.18	3.38	33.24
6.71	-2.73	5.22	3.39	34.10
6.94	-2.73	5.41	3.41	38.15
6.97	-2.73	5.43	3.41	38.56
7.27	-2.73	5.62	3.44	41.46
7.57	-2.73	5.73	3.48	42.69

A Test of the Flashblindness Recovery Functions

The three functions, with parameters derived from flash energy, were fit again to the Smith (1996) data and one other data set from a study by Menendez and Garcia (1985). The latter study was chosen because it employed a similar methodology to the Smith (1996) study. Menendez and Garcia used a single flash energy of 6.7 log td·s, an energy also used by Smith (1996), and both used a uniform, spatially extended source, and a Maxwellian-view system. It would be expected that the decay functions from both studies would have the same time course.

The Menendez-Smith, Smith, and Hahn-Geisler functions were plotted against the Smith (1996) flashblindness recovery data. Some of these plots are shown in Figure 13. Each plot represents one flash energy. The fits to the other flash energies are shown in Appendix C. The Smith and the Hahn-Geisler functions provided good fits to the Smith (1996) data. The Menendez-Smith function, on the other hand, frequently overestimated or underestimated the data. This was probably due to the use of a log-linear function to estimate the offset parameter, c , which means that it continued to increase with flash energy (see Figure 9). The parameters of the other two functions asymptote at higher flash energies (see Figure 11 and Figure 12). The asymptotic behavior of these parameters follows from the limit of flash energy on photopigment bleaching. The parameters should start to asymptote as flash energy approaches 7.6 log td·s as no further bleaching occurs and the light-adapted state of the retina has reached a maximum.

The three functions were plotted against data from the Menendez and Garcia (1985) study. These data, shown in Figure 14, allowed for an unbiased test of the functions because they were not used in parameterization processes. The Smith and Hahn-Geisler functions fit the best. The Menendez-Smith function tended to underestimate recovery times, particularly when the EBL decayed to a very low level.

Based on the foregoing tests, the performances of the Smith and Hahn-Geisler functions were too similar to pick one function over the other. However, upon further examination it became apparent that one function performed better than the other. The Smith function was more robust in that it readily extrapolated to flash energies outside the range used to parameterize the function. For example, Smith (1996) investigated flashblindness recovery to lower flash energies in a chopped pulse experiment. He found that the Smith function accurately predicted up to 1-s of flashblindness, however, when we tested the Hahn-Geisler model, it did not predict any.

Furthermore, the Hahn-Geisler function had some trouble predicting recovery times beyond the flash energy range for which the function was parameterized. The reason for this lack of generality can be found in the equation used to parameterize the time constant (see Figure 12). The time constant, t_c , tails off to zero by the time the flash energy reaches 4.5 log td·s. It is clear that the t_c tapers off too quickly, as it should not have reached zero until the exposure reached 0 log td·s. This behavior of the Gaussian function was probably due to the lack of data points at lower flash energies. If some data were collected at flash energies below 5.4 log td·s, then the cumulative Gaussian would have tapered off more gradually. When future studies provide data at lower flash energies, the Hahn-Geisler function may yet prove to be a viable predictor of flashblindness

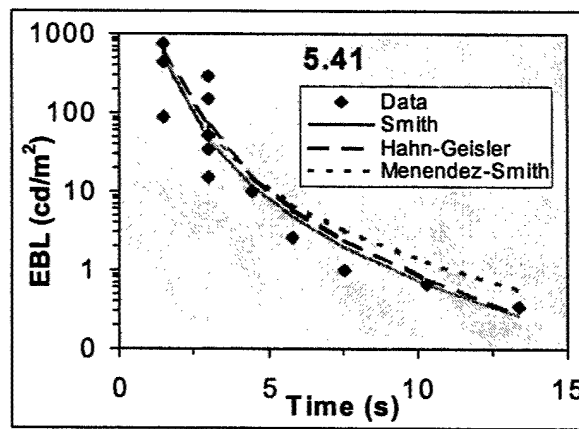
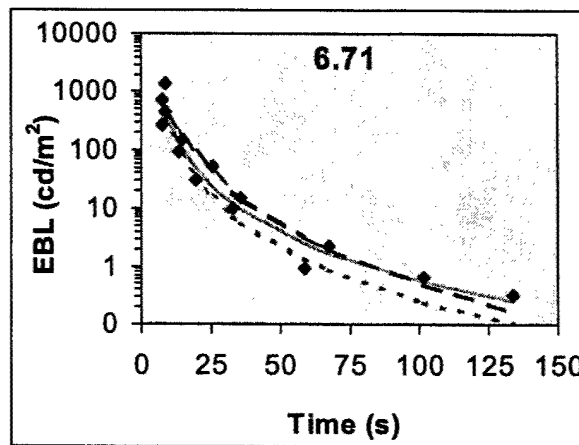
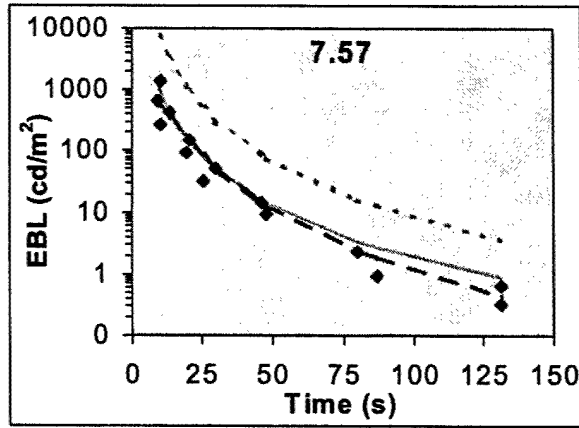


Figure 13. The fit of the three functions to the Smith (1996) flashblindness recovery data for three flash energies. Flash energy is noted at the top of each plot. The Smith is the solid line, the Hahn-Geisler function is the broken line and the Menendez-Smith function is the dotted line.

recovery. At the present time, the Smith function provided the most accurate predictions across a wide range of flash energies and is, therefore, adopted for LTMC.

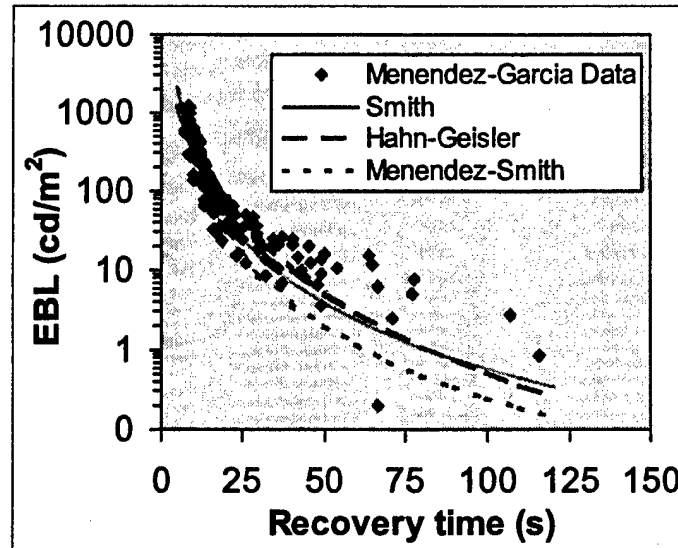


Figure 14. The three decay functions are plotted against the Menendez and Garcia (1985) flashblindness recovery data. The Smith (solid line) and Hahn-Geisler (broken line) functions give the best fits. The Menendez-Smith (dotted line) function underestimates recovery time compared to the other two, especially at low EBLs.

Summary

This report described the status of flashblindness and glare modeling at AFRL/HEDO. The rationale guiding the models' development and the underlying mathematical functions were presented and were supported by the pertinent scientific literature. These models predict the size and/or duration of temporary visual scotomas resulting from optical radiation exposure. The basic components of the models were described. Those components included the wavelength, pulse-width, and irradiance of the laser source, the target and background parameters, and the optical and adaptation state of the eye. Three candidate flashblindness recovery functions were reviewed. The candidate functions were tested against an independent flashblindness recovery data set to determine which function best fit the available data. A function by Smith (1996) was found to be the best performing function.

The following specifications are adopted for the LTMC Glare and Flashblindness Models:

- Glare is defined as an exposure that appears continuous for at least one second.
- The maximum light adaptation effect of the glare source is limited to 7.6 log td.
- Exposure intensity alone determines perceived brightness for exposure durations beyond one second.

- The Flashblindness Model is limited to analyzing exposures 150 ms or less.
- The maximum light adaptation effect of a flashblinding source is limited to $7.6 \log t \cdot s$.
- The Flashblindness Model is limited to analyzing single-pulse exposures (or multiple pulses within 150 ms).
- The Flashblindness Model uses the Smith (1996) function for predicting the time course of flashblindness recovery.
- The minimum predicted flashblindness recovery time is one second.
- Exposure energy and EBL brightness follow the reciprocity law for exposures up to 150 ms.
- Both Models are limited to analyzing point source exposures.
- Both Models are limited to analyzing single wavelength exposures.
- Both models use the TNO point spread function to estimate intraocular light scatter.
- Both models use the photopic spectral luminosity function to correct for the wavelength sensitivity of the eye.

Recommendations

The following recommendations are provided to guide future modeling efforts:

- The TNO algorithm for estimating the retinal light distribution of extended light sources should be included to account for light scattering by optical media such as canopies and windscreens.
- The Flashblindness Model is designed to analyze point sources, but the flashblindness recovery function was developed and validated on data from extended source exposures. The flashblindness recovery function should be re-validated using point source exposures.
- A multiple pulse model should be developed to predict the effect of cumulative pulses on the light adaptation level of the visual system.
- Experiments should be conducted to resolve reciprocity issues for exposures between 10 ms and one second.
- The model should be enhanced to allow independent positioning of the target and light source to fall anywhere on the retina.
- The model should be enhanced by adding targets to the database that involve critical flying tasks, especially those involving HUD symbology.

References

- Akerman III, A., & Kinzly, R. E. 1979. Predicting aircraft detectability. *Human Fac.*, 21, 277-291.
- American National Standards Institute. 2000. *American National Standard for Safe Use of Lasers*. (Standard Z136.1). Orlando, FL: The Laser Institute of America.
- Barlow, H.B. 1958. Temporal and spatial summation in human vision at different background intensities. *J. Physiol.*, 141, 337-350.
- Barlow, H.B. & Sparrock, J.M.B. 1964. The role of afterimages in dark adaptation. *Science*, 144, 1309-1314.
- Berg, T.J.T.P. van den. 1995. Analysis of intraocular straylight, especially in relation to age. *Optom. Vis.*, 72, 52-59.
- Blick, D.W., Beer, J.M.A., Kosnik, W.D., Troxel, S., Toet, A., Walraven, J., & Mitchell, W. 2001. Laser Glare in the Cockpit: Psychophysical Estimates versus Model Predictions of Veiling Luminance Distribution. *Applied Optics*, 40, 1715-1726.
- Bowie, W.H., & Collyer, S.C. 1973. *Experimental Investigation of Flashblindness Parameters*. DNA 2982F, Washington, D.C.: Defense Nuclear Agency
- Brindley, G.S. 1952. The Bunsen-Roscoe law for the human eye at very short durations. *J. Physiol.*, 118, 135-139.
- Brindley, G. S. 1960. *Physiology of the Retina and Visual Pathway*. London: Edward Arnold.
- Campbell, F.W. & Green, D.C. 1966. Optical and retinal factors affecting visual resolution. *J. Physiol.*, 181, 576-593.
- Campbell, F.W. & Gubisch, R.W. 1966. Optical quality of the human eye. *J. Physiol.*, 186, 558-578.
- Chisum, G.T. 1973. Flashblindness recovery following exposure to constant energy adaptive flashes. *Aerosp. Med.*, 44, 407-413.
- Cobb, P.W. 1911. The influence of illumination of the eye on visual acuity. *Am. J. Physiol.*, 29, 76-99.
- Commission Internationale de l'Eclairage. 1926. *CIE Proc.*, 1924, Cambridge, England: Cambridge University Press.
- Crawford, B.H. 1937. The change of visual sensitivity with time. *Proc. Roy. Soc.*, B123, 69-89.
- Crawford, B.H. 1946. Photochemical laws and visual phenomena. *Proc. Roy. Soc.*, B133, 63-75.
- Crawford, B.H. 1947. Visual adaptation in relation to brief conditioning stimuli. *Proc. Roy. Soc.*, B134, 283-302.
- de Groot, S.E. & Gebhard, J.W. 1952. Pupil size as determined by adapting luminance. *J. Opt. Soc. Am.*, 42, 492-495.

- Hahn, L.W. & Geisler, W.S. 1995. Adaptation mechanisms in spatial vision. I. Bleaches and backgrounds. *Vis. Res.*, 35, 1585-1594.
- Hollins, M. & Alpern, M. 1973. Dark adaptation and pigment regeneration in human cones. *J. Gen. Physiol.*, 62, 430-447.
- Hood, D.C. & Finkelstein, M.A. 1986. Sensitivity to light. In K.R. Boff, L. Kaufman, and J.P. Thomas (Eds.), *Handbook of Perception and Human Performance, Vol. I, Sensory Processes and Perception*. Ch. 5, 1-66. New York: Wiley and Sons.
- Ijspeert, J.K., Berg, T.J.T.P. van den, & Spekreijse, H. 1993. An improved mathematical description of the foveal visual point spread function with parameters for age, pupil size, and pigmentation. *Vis. Res.*, 30, 699-707.
- Ijspeert, J.K., Waard, P.W.T. de, Berg, T.J.T.P. van den, & Jong, P.T.V.M. de. 1990. The intraocular straylight function in 129 healthy volunteers: Dependence on angle, age and pigmentation. *Vis. Res.*, 30, 699-708.
- Irving, D. 1960. *The Optical Blink Reaction Time*. Air Ministry FPRC Memo 101, Farnborough, U.K.: Ministry of Defence.
- Jennings, J.A.M., & Charman, W.N. 1981. Off-axis quality in the human eye. *Vis. Res.*, 21, 445-456.
- Karn, H.W. 1936. Area and the intensity-time relation in the fovea. *J. Gen. Physiol.*, 14, 360-369.
- Kosnik, W.D. 1988. *A Preliminary Model of the Distribution of Laser-induced Retinal Lesions Resulting from Eye and Head Responses*. USAFSAM-TR-87-17. Brooks Air Force Base, TX: USAF School of Aerospace Medicine.
- Kosnik, W.D. 1997. *Reciprocity of Intensity and Duration on the Dark Adaptation Effects of Light Pulses*. Unpublished report.
- Kosnik, W.D., & Kang, R. 1998. *An Examination of the Validity of the Equivalent Background Principle for Predicting Optical Radiation Flashblindness Effects*. AL/OE-TR-1997-0176. Brooks Air Force Base, TX: USAF Armstrong Laboratory.
- Lamar, E.S., Hecht, S., Hendley, C.D., & Shlaer, S. 1948. Size, shape, and contrast in detection of targets by daylight vision: II. Frequency of seeing and the quantum theory of cone vision. *J. Opt. Soc. Am.*, 38, 741-755.
- Lamar, E.S., Hecht, S., Shlaer, S., & Hendley, C.D. 1947. Size, shape, and contrast in detection of targets by daylight vision: I. Data and analytical description. *J. Opt. Soc. Am.*, 37, 531-545.
- Meeteren, A., van. 1974. Calculations on the optical modulation transfer function of the human eye for white light. *Opt. Acta*. 21, 395-412.
- Mellerio, J., Marshall, J., Tengroth, B., Anderberg, B., & Wolbarsht, M. 1991. Battlefield laser weapons: an assessment of systems, hazards, injuries and ophthalmic resources required for treatment. *Lasers Light Ophthalmol.*, 4, 41-67.

- Menendez, A.R. & Garcia, P.V. (1985). Human Psychophysics—contrast sensitivity measures of flashblindness. In J.A. Zuclich, R.D. Glickman, F.H. Previc, A.R. Menendez, J.C. Brakefield, M.F. Blankenstein, P.V. Garcia, A.J. Catalano, W.R. Elliott III, and D.J. Coffey. *Effects of Laser Radiation on the Eye: Volume IV*. USAFSAM-TR-85-13. Brooks Air Force Base, TX: USAF School of Aerospace Medicine.
- Menendez, A.R. & Smith, P.A. 1990. Model for predicting the effects of laser exposures and eye protection on vision. In *Laser Safety, Eyesafe Laser Systems, and Laser Eye Protection, SPIE Proc., 1207*, 21-33.
- Miller, N.D. 1965. Visual recovery from brief exposures to high luminance. *J. Opt. Soc. Am.*, 55, 1661-1669.
- Miller, N.D. 1966a. Positive afterimage following brief high-intensity flashes. *J. Opt. Soc. Am.*, 56, 802-806.
- Miller, N.D. 1966b. Positive afterimage as a background luminance. *J. Opt. Soc. Am.*, 56, 1616-1620.
- Miller, N.D., King, V.M., & Schoessler, J. 1968. *Visual Performance Following High Intensity Flashes*. Columbus, Ohio: The Ohio State University Research Foundation.
- Pokorny, J., & Smith, V.C. 1986. Colorimetry and Color Discrimination. In K.R. Boff, L. Kaufman, and J.P. Thomas (Eds.), *Handbook of Perception and Human Performance, Vol. I, Sensory Processes and Perception*. Ch. 8, 1-51. New York: Wiley and Sons.
- Previc, F.H. 1987. Color-specific effects of intense laser exposure on visual evoked potentials in rhesus monkeys. *Aviat. Sp. Environ. Med.* 58, 1103-1108.
- Rushton, W.A.H. 1964. Flash photolysis in human cones. *Photochem. Photobio.*, 3, 561-577.
- Rushton, W.A.H., & Henry, G.H. 1968. Bleaching and regeneration of cone pigments in man. *Vis. Res.*, 8, 617-631.
- Schmeisser, E.T. 1987. *Laser Flash Effects on Chromatic Discrimination in Monkeys*. USAFSAM-TR-87-17. Brooks Air Force Base, TX: USAF School of Aerospace Medicine.
- Scott, W.B. 1999. Beam weapons edging into arsenal. *Aviat. Wk. Space Tech.*, 53-55.
- Sliney D.H. & Wolbarsht, M.L. 1985. *Safety with Lasers and Other Optical Sources*. New York: Plenum.
- Sloan, L.L. 1961. Area and luminance of test objects as variables in examination of the visual field by projection perimetry. *Vis. Res.*, 1, 121-138.
- Smith, P.A. 1996. *A Study of the Transient Effects of High Energy Laser Light on Visual Function*. Unpublished Doctoral Dissertation, University of London.
- Sperling, H.G., & Jolliffe, C.L. 1965. Intensity-time relationship at threshold for spectral stimuli in human vision. *J. Opt. Soc. Am.*, 55, 191-199.

- Stamper, D.A., Lund, D.J., Molchany, J.W., & Stuck, B.E. 2000. Laser-induced afterimages in humans. *Percept. Mot. Skil*, 91, 15-33.
- Stewart, B.R. 1972. Temporal summation during dark adaptation. *J. Opt. Soc. Am.*, 62, 449-457.
- Toet, A., Ijspeert, J.K., & Walraven, J. 1995. *Computing the retinal image profile*. TNO-TM 1995 C-35, TNO Human Factors, Soesterberg, The Netherlands
- Varner, D.C., Cartledge, R.M., Elliott III, W.R., Menendez, A.R., Carrier, and R., Richter, M.J. 1988. *Wavelength-dependent and -independent Effects of Veiling Glare on the Visibility of Head-up display (HUD) Symbology*. USAFSAM-TR-88-15. Brooks Air Force Base, TX: USAF School of Aerospace Medicine.
- Vos, J.J. 1963. Contribution of the fundus oculi to entoptic scatter. *J. Opt. Soc. Am.*, 53, 1449-1451.
- Vos, J.J. 1984. Disability glare – a state of the art report. *CIE J.*, 3, 39-53.
- Vos, J.J., & Berg, T.J.T.P., van den. 1997. On the course of the disability glare function and its attribution to components of ocular scatter. *CIE TC 1-18 Chairman's Report*, 124, 11-29.
- Watson, A.B. 1986. Temporal sensitivity. In K.R. Boff, L. Kaufman, & J.P. Thomas (Eds.), *Handbook of Perception and Human Performance, Vol. I, Sensory Processes and Perception*. Ch. 6, 1-43. New York: Wiley and Sons.
- Westheimer, G. 1986. The eye as an optical instrument. In K.R. Boff, L. Kaufman, & J.P. Thomas (Eds.), *Handbook of Perception and Human Performance, Vol. I, Sensory Processes and Perception*. Ch. 4, 1-20. New York: Wiley and Sons.
- Wooten, B.R. & Geri, G.A. 1987. Psychophysical determination of intraocular light scatter as a function of wavelength. *Vis. Res.* 27, 1291-1298.

Appendix A

Recovery time (s) data versus the EBL ($\text{cd}\cdot\text{m}^2$) at ten laser energy levels (log td·s) from Smith (1996).

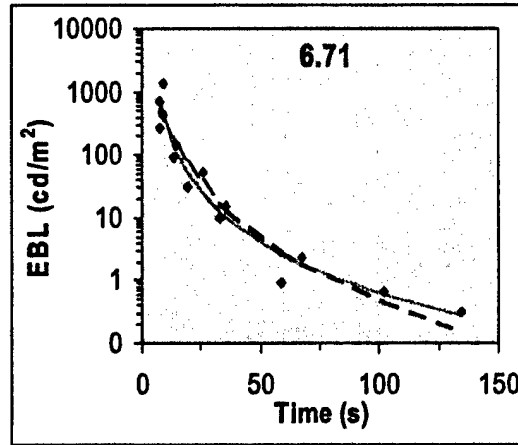
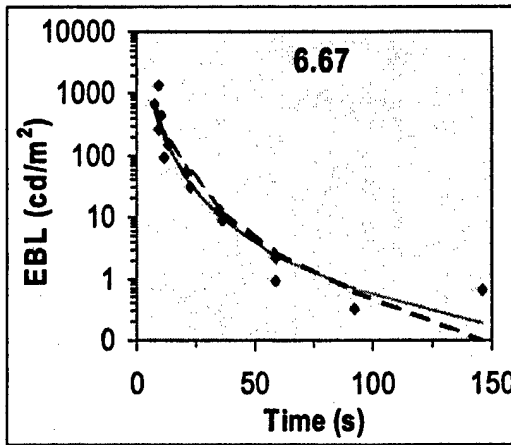
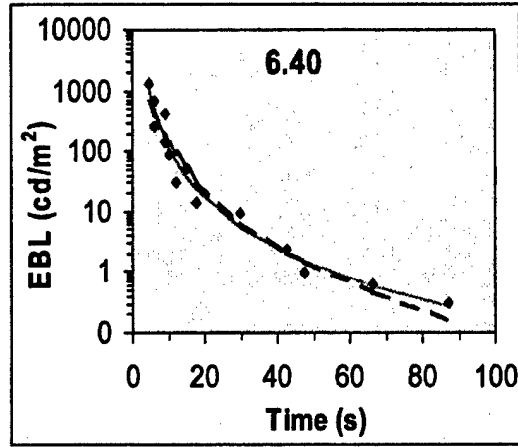
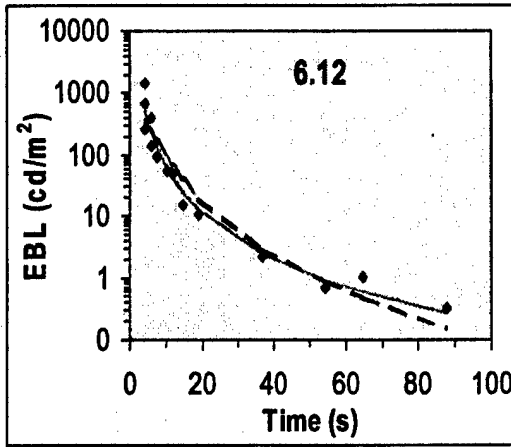
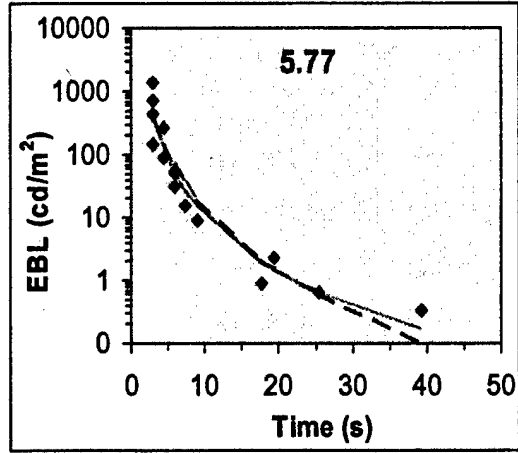
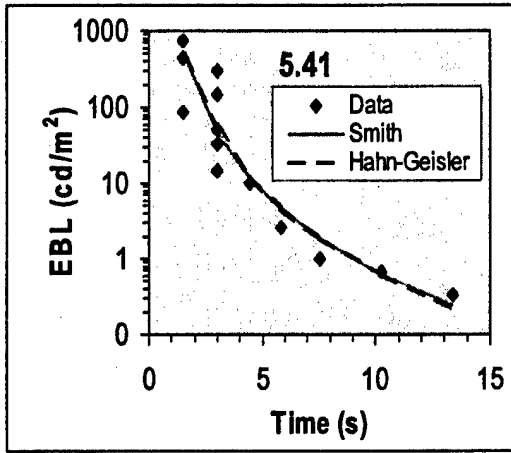
5.41 log td's		5.77 log td's		6.12 log td's		6.40 log td's	
Time (s)	EBL	Time (s)	EBL	Time (s)	EBL	Time (s)	EBL
1.5	1501.3	3.0	1389.5	4.5	1436.5	4.5	1317.4
1.5	762.7	3.0	719.7	4.5	661.0	6.1	688.7
1.5	443.7	3.0	439.4	4.5	267.3	6.1	260.3
1.5	87.3	3.0	150.9	5.9	394.0	9.0	423.4
3.0	295.5	4.5	268.3	5.9	140.0	9.0	147.6
3.0	150.1	4.5	92.1	7.4	95.0	10.3	90.7
3.0	50.8	5.9	51.8	10.4	56.6	12.1	30.4
3.0	33.8	5.9	31.6	11.9	49.7	15.1	51.4
3.0	15.0	7.4	15.1	14.8	15.5	17.8	14.1
4.5	10.0	9.0	9.2	19.2	10.5	29.9	9.4
5.8	2.6	17.8	0.9	36.8	2.2	42.8	2.4
7.6	1.0	19.3	2.3	54.4	0.7	47.7	1.0
10.3	0.7	25.4	0.7	64.8	1.0	66.3	0.6
13.4	0.3	39.4	0.3	87.8	0.3	87.2	0.3

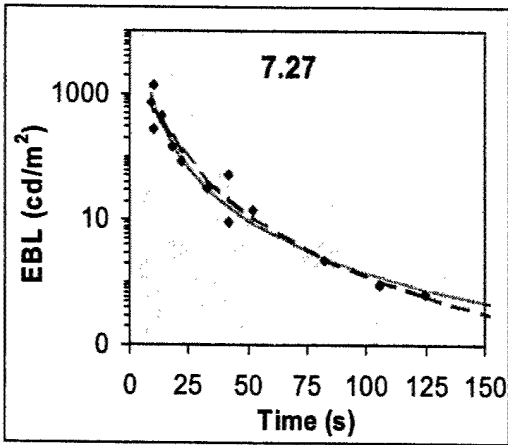
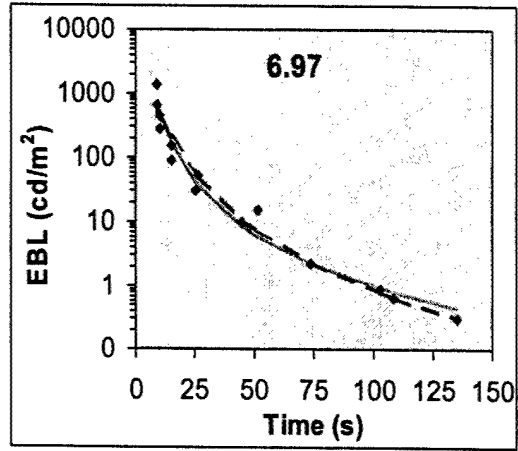
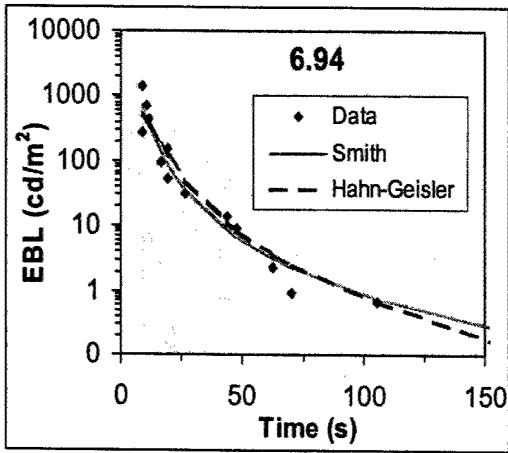
6.67 log td's		6.71 log td's		6.94 log td's		6.97 log td's	
Time (s)	EBL	Time (s)	EBL	Time (s)	EBL	Time (s)	EBL
7.5	662.9	7.5	719.7	9.0	1389.5	9.0	1389.5
9.0	1389.5	7.5	268.3	9.0	268.3	9.0	662.9
9.0	268.3	9.0	1389.5	10.3	719.7	10.3	439.4
10.4	439.4	9.0	439.4	11.8	439.4	10.3	277.2
11.9	92.1	13.7	92.1	16.4	92.1	15.1	150.9
13.7	150.9	14.8	150.9	19.3	150.9	15.1	92.1
20.6	51.8	19.5	31.6	19.3	51.8	25.4	31.6
22.4	31.6	25.7	51.8	26.8	31.6	26.8	51.8
34.8	13.9	33.0	10.0	43.9	13.9	45.2	10.0
35.8	9.2	35.8	15.1	47.7	9.2	51.8	15.1
58.7	2.3	58.7	0.9	62.8	2.3	74.0	2.3
58.7	0.9	67.4	2.3	70.0	0.9	102.8	0.9
92.5	0.3	101.9	0.7	105.6	0.7	108.6	0.7
145.7	0.7	134.1	0.3	170.7	0.3	135.2	0.3

7.27 log td·s		7.57 log td·s	
Time (s)	EBL	Time (s)	EBL
9.0	719.7	9.0	662.9
10.3	1389.5	10.3	1389.5
10.3	268.3	10.3	268.3
13.5	439.4	13.5	439.4
17.8	138.9	19.3	92.1
22.1	84.8	20.7	150.9
32.5	31.6	25.4	31.6
41.6	51.8	29.9	51.8
41.6	9.2	45.8	13.9
51.8	13.9	47.7	9.2
82.5	2.3	80.3	2.3
105.6	0.9	87.2	0.9
124.5	0.7	131.5	0.7
159.4	0.3	131.5	0.3

Appendix B

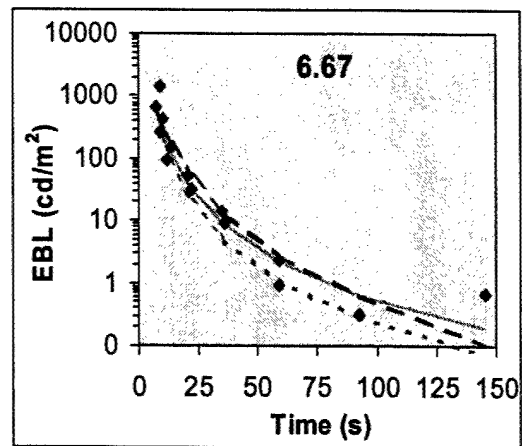
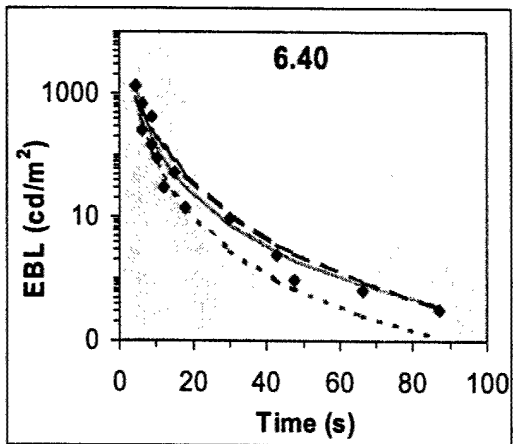
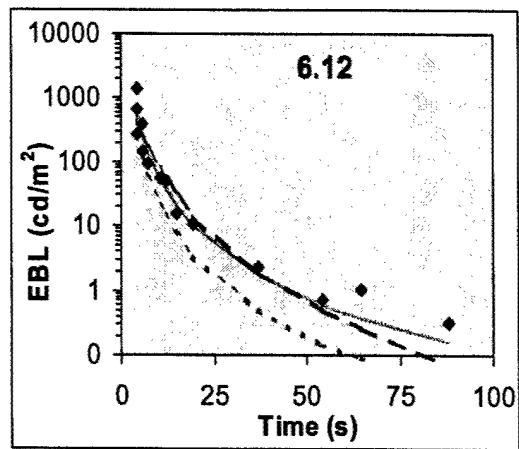
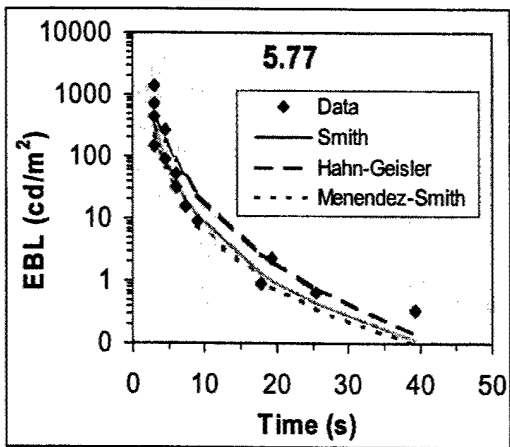
Plots of the Smith (solid line) and Hahn-Geisler (broken line) functions fitted to the Smith (1996) data (symbols; see Appendix A), using the empirically derived parameters. The data are given in recovery time versus the *EBL*. Flash energies in log td's are reported at the top of each figure.

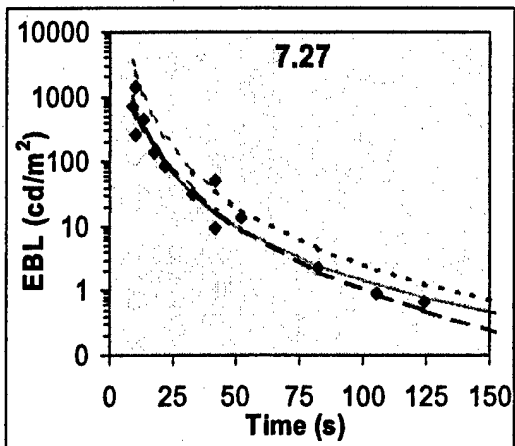
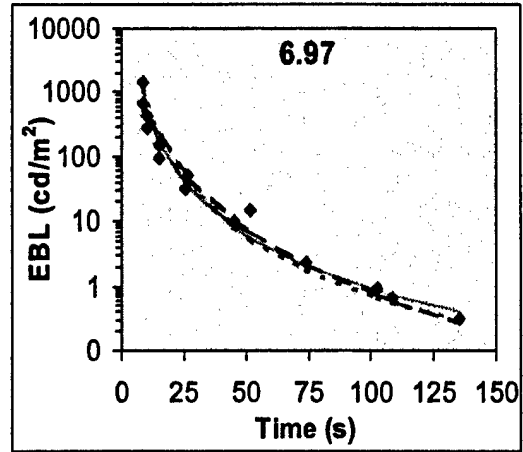
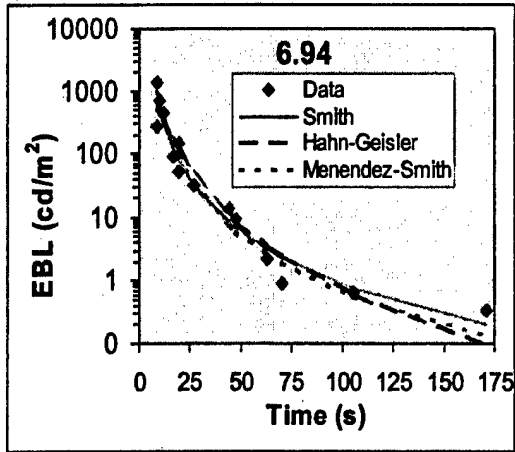




Appendix C

Plots of the Smith (solid line), Hahn-Geisler (broken line), and Menendez-Smith (dotted line) functions fitted to the Smith, 1996, data using the parameters derived from the flash energies. The data are given in recovery time versus the *EBL*. Flash energies in log td's are reported at the top of each figure.





Appendix D

Data from Menendez and Garcia (1985) showing the recovery time vs. the EBL. The raw data were transformed into EBLs from contrast scores. Data are from four observers and five sine wave gratings, 1,4,8,12, and 24 $\text{c}\cdot\text{d}^{-1}$. Each score represents the average from ten flash recovery trials.

Recovery time (s)	EBL (cd·m ⁻²)
6	1180
7	552
7	575
8	589
8	585
8	830
8	1240
8	933
8	287
9	271
9	790
9	282
9	578
9	1153
9	990
9	480
10	160
10	648
10	138
10	615
10	410
10	288
10	571
10	500
11	289
11	390
11	136
11	490
11	462
11	235
12	284
12	427
12	281
12	130
12	303
12	319
12	154
12	245
12	145
13	113
13	64
13	226
13	240
13	190

Recovery time (s)	EBL (cd·m ⁻²)
13	140
13	200
14	208
14	73
14	66
14	141
14	137
14	118
15	153
15	63
15	85
15	120
16	83
16	99
16	113
16	33
16	68
16	54
17	94
17	76
17	99
17	56
17	29
18	37
18	90
19	61
19	60
19	66
19	24
20	35
20	70
21	54
21	43
21	65
21	57
22	65
22	38
22	47
22	29
23	33
23	32
23	31
23	16
25	25

Recovery time (s)	EBL (cd·m ⁻²)
26	50
26	12
27	38
27	40
28	47
28	37
29	29
29	36
29	26
30	24
30	19
31	19
32	9
32	14
34	25
34	25
34	20
34	12
34	21
36	21
36	11
37	27
37	7
40	25
40	21
42	14
43	10
44	8
45	20
46	12
48	7
49	14
49	4
49	9
50	16
54	11
64	15
65	12
67	0
67	6
71	3
77	5
78	8
107	3